ARTICLES

Journal of Semiconductors
(2022) 43, 092302
doi: 10.1088/1674-4926/43/9/092302

Organic bulk heterojunction enabled with nanocapsules of hydrate vanadium pentaoxide layer for high responsivity self-powered photodetector

Hemraj Dahiya[1], Anupam Agrawal[2], Ganesh D. Sharma[1], and Abhishek Kumar Singh[3, †]

[1]The LNM Institute of Information Technology, Department of Physics, Jaipur, Rajasthan 302031, India

[2]Bhilai Institute of Technology, Durg, Chhattisgarh, 491001, India

[3]Rajiv Gandhi Institute of Petroleum Technology, Department of Electronics Engineering , Amethi, U.P. 229304, India

Abstract: This article demonstrates the fabrication of organic-based devices using a low-cost solution-processable technique. A blended heterojunction of chlorine substituted 2D-conjugated polymer PBDB-T-2Cl, and $PC_{71}BM$ supported nanocapsules hydrate vanadium penta oxides (HVO) as hole transport layer (HTL) based photodetector fabricated on an ITO coated glass substrate under ambient condition. The device forms an excellent organic junction diode with a good rectification ratio of ~200. The device has also shown excellent photodetection properties under photoconductive mode (at reverse bias) and zero bias for green light wavelength. A very high responsivity of ~6500 mA/W and high external quantum efficiency (EQE) of 1400% have been reported in the article. The proposed organic photodetector exhibits an excellent response and recovery time of ~30 and ~40 ms, respectively.

Key words: self-powered detector; green light sensor; HVO; PBDB-T-2Cl detector; processable solution sensor

Citation: H Dahiya, A Agrawal, G D Sharma, and A K Singh, Organic bulk heterojunction enabled with nanocapsules of hydrate vanadium pentaoxide layer for high responsivity self-powered photodetector[J]. *J. Semicond.*, 2022, 43(9), 092302. https://doi.org/10.1088/1674-4926/43/9/092302

1. Introduction

Photodetectors (PDs), which serve as a practical technological device for converting the absorbed optical energy into electrical signals, have gained considerable interest. They are helpful in several scientific and industrial applications, such as light-wave communications, military affairs, medical diagnostic, biological sensors, optical surveillance, physical sensors, biochemical detection, and image sensing, etc.[1–10]. The commercial market of PDs is still dominated by inorganic semiconductor-based PD such as germanium, silicon, and III–V group elements owing to their excellent mobility of charge carriers, the small binding energy of exciton, high durability, and robustness[11–15]. However, inorganic-based PD has several drawbacks, such as complex and costly fabrication processes and non-eco-friendly and mechanical rigidity restricting their application in portable and flexible systems.

Over the last two decades, organic PDs (OPDs) have gained even more interest due to their unique benefits over conventional-based PD, such as transparent, flexible, lightweight, adjustable energy levels, large scale possibility, low cost, chemically tailoring and structural diversity, etc.[16–27]. Most of the organic semiconductor materials and, therefore, efficient charge extraction through continuous transport pathways. For the optimal performance of OPDs, proper selection of weight ratio of the acceptor and donor is essential for the better external quantum efficiency (EQE), energy level tuning, and photo-multiplication characteristics of the PDs[19, 20, 28, 29]. Several donor and acceptor materials have been used for the PDs applications, such as P3HT, ITIC, MEH-PPV, PTB7-Th, PQT-12, $PC_{61}BM$, $PC_{71}BM$, PSBTBT-NH2, F8BT, and PDTSTPD, etc. The journey of OPD begun in 1981, when Kudo and Moriizumi reported the first organic OPDs having structure ITO/ merocyanine dye/rhodamine B dye/Al. This OPD was prepared in a vacuum by a sublimation process that demonstrated a spectral response range only in the visible spectrum region[30]. In 1993, the first MEH-PPV and C60 based planar heterojunction polymer photodiodes were established by Sariciftci and his team[31]. Furthermore, in 1995 concept of bulk heterojunction (BHJ) diodes consists of the blend of polymer-polymer and polymer–fullerene was realized[32, 33]. The enhancement of OPDs performance is accomplished by considering the device's architecture engineering and the photoconductive layer's materials engineering. Improvements in OPD performance using new design strategy in materials and their optimized arranging in various device architectures have been continued and showed some practical application. Rauch *et al.* prepared hybrid OPD (for near-infrared imaging) based on the P3HT/PCBM blend added with PbS quantum dot, delivering 51% of EQE and fast temporal response of fewer than 100 μs[34]. Han *et al.* exhibited ambient light oximeter OPD with two different blends: PCDTBT/$PC_{71}BM$ and P3HT:O-IDTBR[35]. Hung *et al.* demonstrated OPD for heart rate monitoring using PTB7-Th/CO1-4CL and achieved an outstanding responsivity of more than 0.5 A/W in the 920–960 nm NIR spectral range[36]. Strobel *et al.* displayed pristine polyindenoflurorene-8-triarylamine (PIF) (polymer donor)/ITIC (non-fullerene acceptors) and PIF (polymer donor)/IDFBR (non-fullerene acceptors) based multichannel visible light communication system with responsiv-

Correspondence to: A K Singh, aks@rgipt.ac.in
Received 26 FEBRUARY 2022; Revised 18 APRIL 2022.

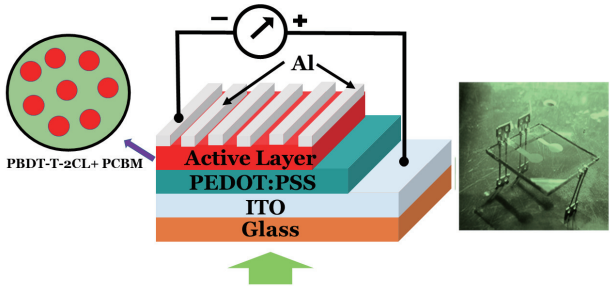

Fig. 1. (Color online) Schematic architecture of organic photodetector and the image of fabricated device.

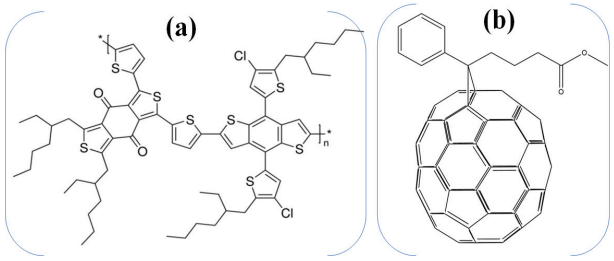

Fig. 2. Chemical structure of (a) PBDB-T-2Cl and (b) $PC_{71}BM$.

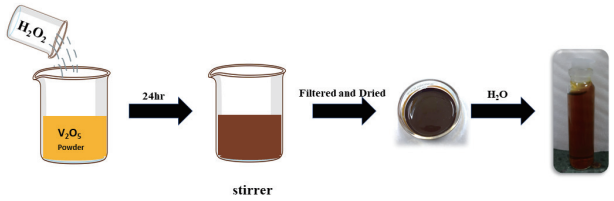

Fig. 3. (Color online) One-step method of synthesis of HVO nanocapsules.

ity greater than 102 mA/W[37]. Kumar *et al.* recently reported a self-powered OPD based on PQT-12/ $PC_{61}BM$ with 41.6% of EQE obtained at 515 nm at 57 $\mu W/cm^2$ and responsivity of approximately 167.5 mA/W[38]. State-of-the-art of OPDs research lacks to achieve a very high responsivity as compared to their inorganic counterpart. In this work, we have fabricated a self-powered photodetector based on PBDB-T-2Cl:$PC_{71}BM$ BHJ active layer employing hydrate vanadium pentaoxide (HVO) nano-capsules as hole transport layer (HTL) and found it operates in the visible region.

2. Experimental section

2.1. Device structure

The low-cost proposed structure with ITO/HVO/ PBDB-T-2Cl: $PC_{71}BM$ /Al is fabricated by depositing the thin film layer on a glass substrate using a solution-processable technique.

In Fig.1(a), the schematic structure and fabricated devices image are respectively. The chemical structure of the active layer materials used in OPD has shown in Fig. 2.

2.2. Device fabrication steps

HVO nano-capsules were synthesized as shown in Fig. 3 by the one-step method[39]. In this method, vanadium pentoxide (V_2O_5) powder (0.5g) (Sigma Aldrich (CAS#223794)) dissolved into 30% hydrogen peroxide (H_2O_2) (Thermo Fisher (CAS#7722-84-1,7732-18-5) solution (50 mL). A reddish-brown precipitate was obtained after the continuous stirring of 24 h at room temperature. Then the filtration is done with high-quality Whatman filter paper, and washing is done using 10%

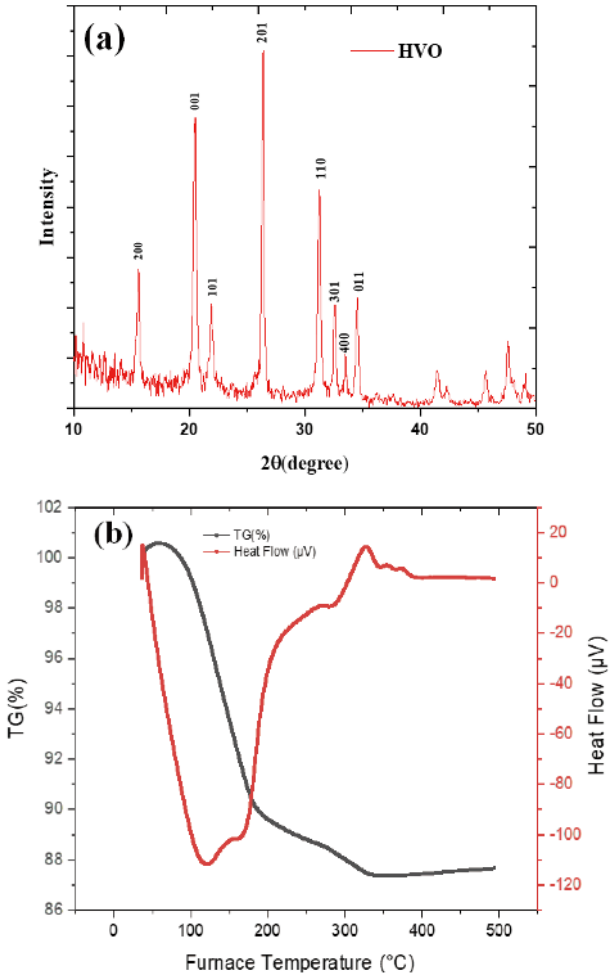

Fig. 4. (Color online) (a) XRD spectra and (b) TGA curve of HVO.

H_2O_2 solution. After the filtration, the residue was kept overnight for room temperature drying and then moved to the furnace to remove water contents at 110 °C for 1 h for the fabrication of HVO/PBDB-T-2Cl:$PC_{71}BM$/Al photodetector device. Before coating HVO, the ITO substrates were cleaned by sequential ultrasonication in dilute detergent solution, deionized (DI) water, acetone, and isopropyl alcohol for 20 min each. The substrate was then dried in an oven at 50 °C for 30 min. The HVO was spin-coated at 3000 r/min for 45 s onto the cleaned ITO substrates and subsequently annealed at 100 °C for 15 min. For the fabrication of photoactive layers composed of electron donor and acceptor, PBDB-T-2Cl (CAS. #2239295-71-5, purchase from Ossila) and $PC_{71}BM$ (CAS#609771-63-3, purchase from Ossila) respectively, use organic materials which were dissolved in chloroform to produce a 1 : 1 solution and followed by shaking at room temperature for 12 h (Total concentration 10 mg/mL). PBDB-T-2Cl:$PC_{71}BM$ thin film was spin-coated at 2000 r/min for 30 s onto the HVO layer, and the film was annealed at 100 °C for 15 min. Finally, a 100 nm thick aluminum (Al) electrode was deposited on the top of the active layer via thermal evaporation at a pressure of less than 10^{-5} Torr. The active area of the cell was 0.205 cm^2.

3. Results and discussion

The X-ray diffraction (XRD) spectrum of HVO illustrates in Fig. 4(a). The diffracted peaks are well-matched with standard JCPDS#96-202-0757 and confirmed the orthorhombic

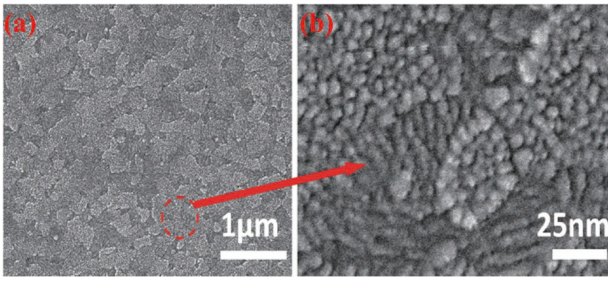

Fig. 5. (a) SEM image of HVO thin film on the scale of 1μm and (b) 25 nm respectively on ITO coated substrate.

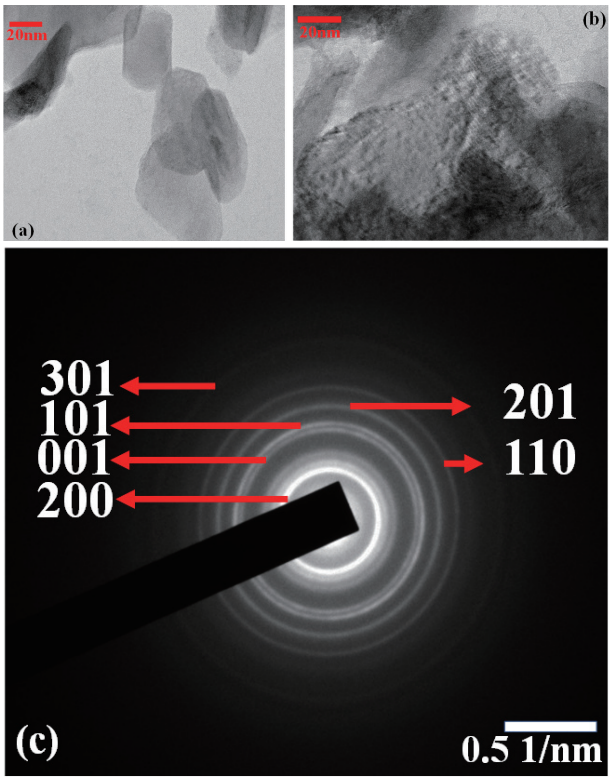

Fig. 6. (a, b) HR-TEM image (scale 20nm). (c) SAED pattern of HVO nano capsule.

(a = 11.51200 Å, b = 3.56400 Å, c = 4.36800 Å,) layered structure of vanadium pentoxide. Also, the narrow and intense diffraction peaks reveal that the HVO nanoparticle was highly crystalline[40]. The average measured crystallite size from the XRD of HVO by using the Debye Scherrer formula was 29.20 nm.

The presence of water molecules in the HVO was investigated by thermogravimetric analysis (TGA) (Fig. 4(b)) using the A-Torracca formula[41]. It is found that the material consists of mostly 1.5 water molecules (calculated total weight loss is 13%), which confirmed the hydrating nature of V_2O_5.

The scanning electron microscope (SEM) of HVO film was displayed in Fig. 5, showing the formation of a tightly bound capsule network. These types of networked morphologies may be suitable enough for the operation of interfacial charge transport in photodiodes. Also, the alignment of HOMO and LUMO energy levels are demonstrated by the efficient charge transport between interfacial layers of in given photodetector[42].

The high-resolution scale transmission electron microscope (HRTEM) is used to get the information about the formation of the HVO nanocapsule, and shown in Fig. 6(a). The HRTEM image in Fig. 6(b), shows the different grain boundaries that confirm the polycrystalline nature of the sample. The selected area electron diffraction (SAED) pattern was shown in Fig. 6(c), which displays the polycrystalline nature of HVO.

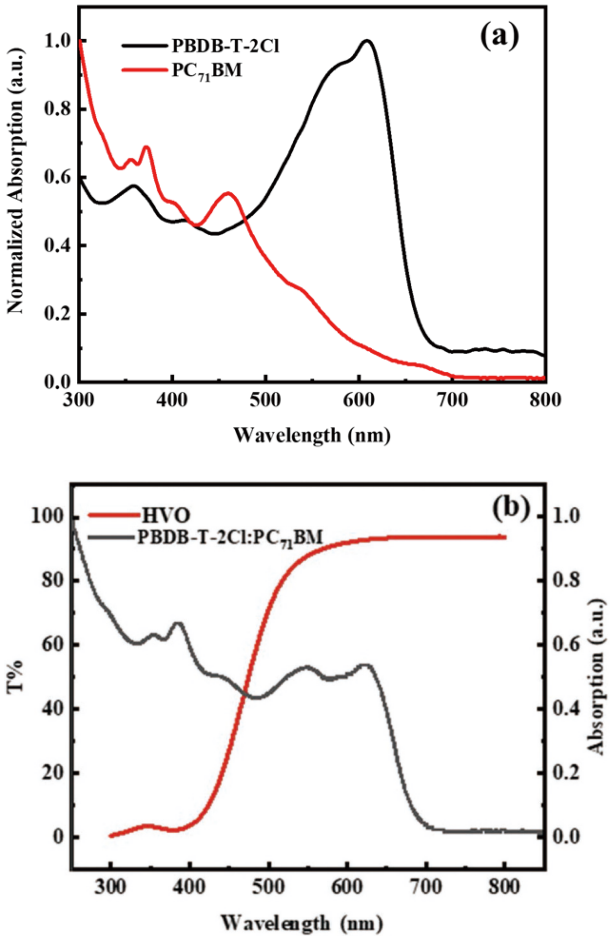

Fig. 7. (Color online) (a) Absorption spectra of PBDB-T-2Cl and $PC_{71}BM$. (b) Transmittance and absorption spectra of HVO and PBDB-T-2Cl: $PC_{71}BM$ blend.

The optical properties of the material are essential when it is used as an active layer for OPD. The UV–vis absorption spectra of pristine PBDB-T-2Cl and $PC_{71}BM$ are shown in Fig. 7(a). The absorption spectra of PBDB-T-2Cl:$PC_{71}BM$ are shown in Fig. 7(b). It can be seen from Fig. 7(b) that the blend showed strong absorption spectra from 300 to 700 nm. The primary purpose of the nanocapsules HVO layer in the detector is: (i) used as an HTL layer for the detector, i.e., it blocks the electron transportation towards the ITO side because of the large barrier height of ~0.93 eV. (ii) It provides a viable path for holes. The active layer of PBDB-T-2Cl:$PC_{71}BM$ blend is suitable for detecting only visible spectrum and showing cut-off for infrared wavelength, i.e., above 700 nm. Therefore, the proposed BHJ-based detector perfectly suits the broadband spectrum of 550 to 625 nm wavelength. Further, we have obtained the optical energy bandgap of 2.48 eV for HVO that shows high transparency to the visible region, as shown in Fig 7(b). The optical energy band gap PBDB-T-2Cl and $PC_{71}BM$, estimated from the onset absorption edge (Fig. 7(a)), is 1.85 and 2.13 eV, respectively. When the light interacts with an active layer of PBDB-T-2Cl:$PC_{71}BM$ blend, the organic molecule of the active layer goes to electron trans-

Table 1. Optical and electrochemical characteristics of polymers.

Polymer	λ_{max} (s) (nm)	λ_{max} (f) (nm)	E_{HOMO} (eV)	E_{LUMO} (eV)	E_g^{ech} (eV)	E_g^{opt} (eV)
PBDB-T-2CL	606	621	−5.32	−3.57	1.75	1.85
$PC_{71}BM$	373, 460	325	−5.90	−3.90	2	2.13

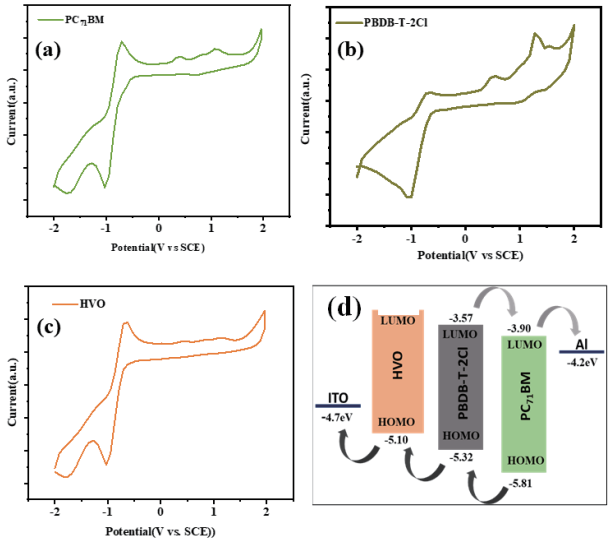

Fig. 8. (Color online) Cyclic voltammetry of (a) HVO, (b) $PC_{71}BM$, and (c) PBDB-T-2Cl. (d) HOMO-LUMO energy level of polymers and charge transfer in the active layer.

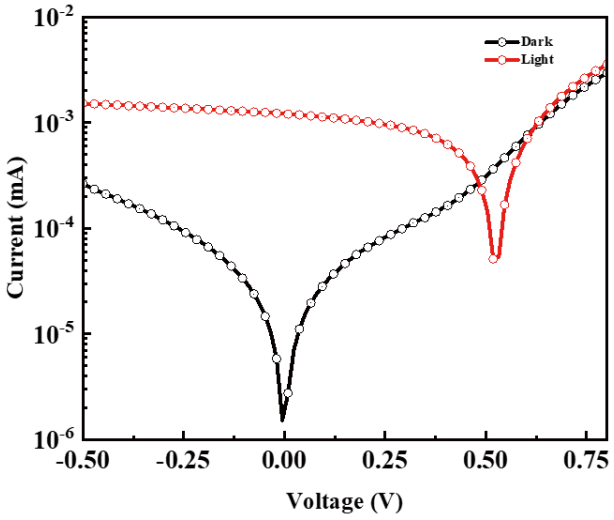

Fig. 9. (Color online) *I–V* characteristics of OPD under dark and illumination

ition, i.e., the electron goes from lower energy to higher energy. Only a fraction of light will be absorbed by the active layer, i.e., the incident light energy must be equal to or more significant than the difference between higher energy levels and the lower energy levels. Therefore, it is essential to find out the energy levels in the active layer of the detector. Also, these energy levels will help us to analyze the charge carrier transport in the photodetector. The investigation of these energy levels, which refers to the highest occupied molecular orbital (HOMO) and lowest unoccupied molecular orbital (LUMO), is essential for HVO and PBDB-T-2Cl:$PC_{71}BM$ for analyzing the electrochemical energy bandgap of material and charge transportation. Electrochemical investigation of HVO

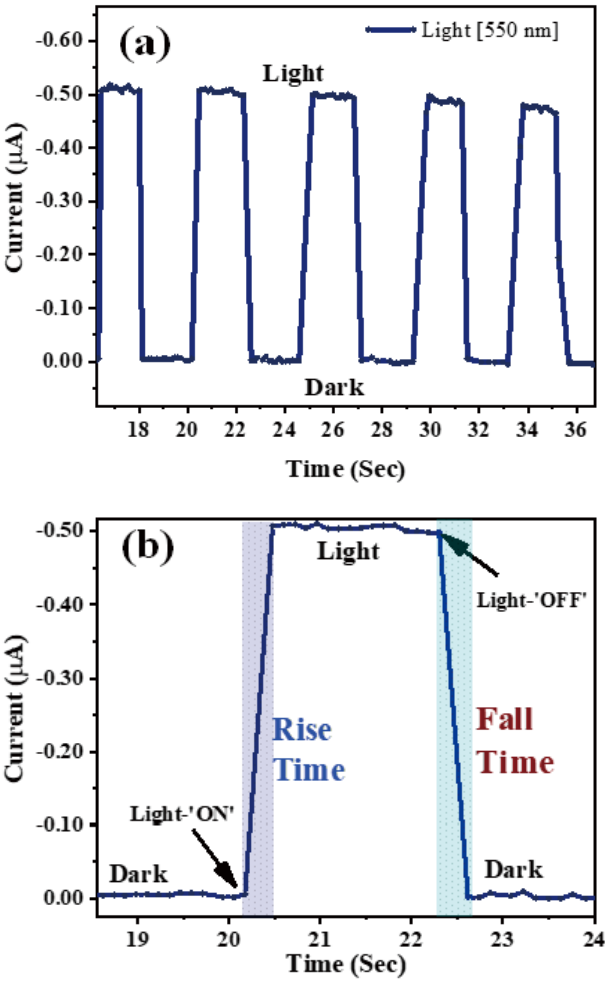

Fig. 10. (Color online) Current time response of the photodetector.

and PBDB-T-2Cl:$PC_{71}BM$ blends were determined by Cyclic Voltammetry (CV) as shown in Fig. 8. We have three electrodes in the CV setup: glassy carbon as working electrode, calomel as reference electrode, and platinum as counter electrodes connected with Keithley 2450. The E_{HOMO} and E_{LUMO} energy levels were estimated via onset oxidation (Ex.) and reduction (Ered.) electrochemical potential, which results are shown in Table 1[43].

The electrical characterization has been carried out by using an Agilent semiconductor parameter analyser in ambient conditions. The diode characteristics of the junction of fabricated structure PBDB-T-2Cl:$PC_{71}BM$ blend, the junction *I–V* characteristics (current-voltage) are shown in Fig. 9.

It shows that the PBDB-T-2Cl as p-type and $PC_{71}BM$ as n-type show a suitable rectifying property. The rectification ratio of the organic junction diode at 1 V is ~250 under dark conditions. The signal to noise ratio i.e., ratio of the photocurrent to the dark current of the self-powered photodetector is found to be ~1000 at 0 V. The current–voltage characteristics of the fabricated detector with the structure ITO/HVO/PBDB-T-2Cl:$PC_{71}BM$/Al under both dark and illumination are investigated at the wavelength of 550 nm, power intensity of 1 mW/cm^2 or 1 Sun. The 550 nm light exposure was used to impose on the backside of the detector from glass/ITO/HVO to the active layer; this wavelength was obtained using a monochromator. The green light has passed through ITO and HVO but is absorbed by the active layer. This can be Green-

Table 2. Comparison table of various self-powered organic based photodetectors.

Entity	Ref. [44]	Ref. [45]	Ref. [30]	Ref. [46]	Ref. [38]	This article
Junction	–	PBDTT-ffQ: $PC_{71}BM$	P3HT:$PC_{71}BM$	PNTT-H: $PC_{71}BM$	PQT-12: $PC_{61}BM$	PBDB-T-2Cl and $PC_{71}BM$
Transportationlayer	ETL:Zr–TiO_x	–	HTL:PEDOT:PSS	HTL:PEDOT:PSS	ETL:ZnO QDs	HTL:HVO nano capsules
Device structure	ITO/PEDOT:PSS/ $CH_3NH_3PbI_xCl_{3-x}$/ $PC_{60}BM$/Zr–TiO_x/Al	PET/PBDTT-ffQ:$PC_{71}BM$/Au	ITO/PEDOT:PSS/ P3HT:$PC_{71}BM$ /Al	ITO/PEDOT:PSS/ PNTT-H:$PC_{71}BM$/ Ca/Al	ZnO QDs/ PQT-12:PC61BM/ MoOx	Glass/ITO/HVO/ PBDB-T-2Cl and $PC_{71}BM$/Al
Self-powered	Yes	Yes	Yes	Yes		Yes
Maximum temp used in fabrication (°C)	130–150	~30	100	100–150	200	100
Operating bias (V)	–0.1	–	–10	–0.1	0	0
Rise time (μs)	0.29	0.0889	–	32	0.07	0.03
Delay time (μs)	0.27	0.0667	–	29	0.1	0.04
Wavelength (nm)	525	365	650	760	515	550
Responsivity (A/W)	0.380	0.115	0.255	0.360	0.1675	6.25
Power density (mW/cm^2)	1 mW/cm^2 = 1 Sun	–	2	–	0.057	1 mW/cm^2 = 1 Sun
EQE (%)	–	–	49 (at 520 nm, –10 V) &53500 (at 620 nm, –60 V)	59.45	41.6	1400 (at 550 nm, 0 V)
NEP (W/(cm^2 · Hz$^{1/2}$))	–	–	–	–	–	2×10^{-11}
Detectivity (10^{11} Jones)	137	6.19	1.3	139	4	40 (0 V, 550 nm)

light interaction with the active layer led to the generation of electron–hole pairs. Once the carrier is generated in the active layer, the proposed support layer is helping to pass these carriers to the respective anode and cathode electrodes. It's interesting to note that the self-powered effect can be seen in Fig 10; the self-powered development enhanced the photogenerated current nearly in the order of ~1000 at the zero bias at a very low intensity of light.

The quantum efficiency of the fabricated detector was calculated using Eq. (1) to define the number of generated photo carriers per photon. The responsivity (R) of an organic photodiode can be defined in Eq. (2) and defined as a ratio of photogenerated current (I_p in A) to the incident power (P in W) at a given wavelength.

$$\eta = \frac{I_p}{q\Phi} = \frac{I_p}{q}\frac{h\nu}{P_{opt}}, \tag{1}$$

$$R_\lambda = \frac{\eta q}{h\nu} = \frac{\eta\lambda\,(\mu\text{m})}{1.24} = \frac{I_p}{P_{opt}} \quad \text{(A/W)}. \tag{2}$$

The figure of merit of photodetector has been evaluated in terms of noise equivalent power (NEP) and detectivity. NEP is defined in Eq. (3) as the minimum optical power at which the signal to noise ratio becomes unity[15, 23–27].

Minimum detectable power (in W/(cm^2·Hz$^{1/2}$)) are obtained with the help of using NEP in terms of Detectivity of the detector as shown in Eq. (4)

$$\text{NEP} = \text{rms optical power } P_{opt}|_{min} = \frac{h\nu}{\eta}\sqrt{\frac{2I_{eq}}{q}}, \tag{3}$$

$$D^* = \frac{\sqrt{A}}{\text{NEP}} \quad \text{Jones}. \tag{4}$$

The photodetector based on the operating voltage is primarily working on the two-mode of operation 1. Photoconductive mode (at revere bias) and 2. Photovoltaic mode (at zero bias). The self-powered detectors do not require any external battery source and could be utilized to measure ambient conditions. This ambient condition can be achieved by measuring the electrical characteristics of the device under natural sunlight. In this article, the organic detector is measured under equivalent to 1 Sun light condition. The proposed organic optical sensor was showing promising results under both modes of operation.

The maximum responsivity and EQE are obtained in the photovoltaic mode of operation under the illumination of the wavelength of 550 nm at power density 1 mW/cm^2. The device shown an excellent result under the photovoltaic mode, i.e., the responsivity and EQE obtained at zero bias is 6.25 A/W and ~1400%. The NEP of the detector is found to be 2×10^{-11} W/(cm^2·Hz$^{1/2}$), and the estimated detectivity of the detector is ~4.0×10^{12} Jones. The current time response is obtained for measuring the detector's response time, as shown in Fig 10. The rise time of the detector is defined as the time required to reach 90% of the steady-state value (final value) from 10% of the initial value, and similar, the fall time was estimated from current changes from 90% of the final value to 10% of the initial value. The estimated rise time and fall time from Fig. 10(b) are 30 and 40 ms, respectively. The detailed performance comparison table of the previously reported organic junction with supporting ETL/HTL based photodiode has been shown in Table 2. The transport mechanism of charge carriers (electrons & holes) of the photodetector[47–53] is shown with the help of energy band diagram in the Fig. 11. As the light incident on the PBDB-T-2Cl/$PC_{71}BM$ BHJ active layer, light having energy greater than bandgap of active layer will be absorbed by active layer, result-

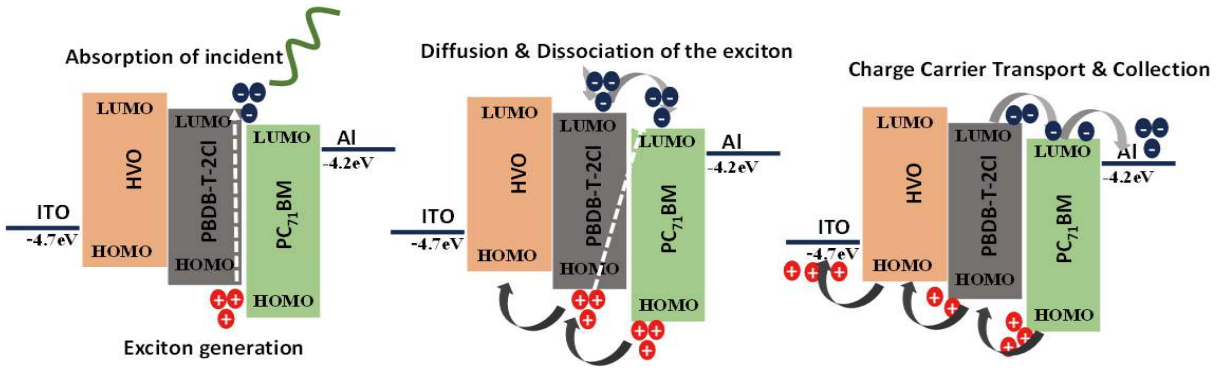

Fig. 11. (Color online) The charge transport mechanism of photodetector.

ing an excition (excite electron from HOMO to LUMO level) generation followed by the excitons diffusion to the donar acceptor interface. At the interface of PBDB-T-2Cl/$PC_{71}BM$, the electron will move to the $PC_{71}BM$ material, and the hole will move from PBDB-T-2Cl to HVO, i.e., the dissociation of the exciton across this interface. HVO layer is used to block the electron from ITO side and make feasible paths for holes. Finally, the charge transfer to the respective electrodes i.e., electrons reached to the Al side and hole reaches to ITO side.

The proposed device achieved excellent detection and responsivity in both photoconductive and photovoltaic modes.

4. Conclusion

In this article, self-powered, a low-temperature processed based organic bulk heterojunction organic photodiode of chlorine substituted 2D-conjugated polymer PBDB-T-2Cl: PCBM is studied over the visible spectrum by using HVO nanocapsules HTL layer. The optical characteristics of the detector have shown an excellent sensing capability at the visible range of 500–625 nm, showing a maximum sensitivity at the wavelength of 550 nm. Further, the electrical characteristics of photodiode were measured using *I–V* characteristics under dark and illumination. The device was intended to make for real-time application because the electrical device characteristics were obtained under natural sunlight, i.e., 1 mW/cm^2. The proposed fabricated device has the highest responsivity of 6250 mA/W at the wavelength of 550 nm at zero bias. The measured NEP and detectivity of the self-powered photodetector are ~2×10^{-12} W/(cm^2·Hz$^{1/2}$) and 4.0×10^{12} Jones respectively. The high responsivity of the self-powered detector can make the device very attractive for real-time batteryless operation

Acknowledgements

Mr. Hemraj Dahiya would like to extend his gratitude to DST, New Delhi for INSPIRE Fellowship (IF190560).

References

[1] Gao Z, Jahed N M S, Sivoththaman S. Large area self-powered Al-ZnO/(n)Si hetero-junction photodetectors with high responsivity. IEEE Photonics Technol Lett, 2017, 29, 1171

[2] Zhang X, Yang S, Zhou H, et al. Perovskite-erbium silicate nanosheet hybrid waveguide photodetectors at the near-infrared telecommunication band. Adv Mater, 2017, 29, 1604431

[3] Upadhyay R K, Singh A P, Upadhyay D, et al. $BiFeO_3/CH_3NH_3PbI_3$ perovskite heterojunction based near-infrared photodetector. IEEE Electron Device Lett, 2019, 40, 1961

[4] Tittl A, Michel A K U, Schäferling M, et al. A switchable mid-infrared plasmonic perfect absorber with multispectral thermal imaging capability. Adv Mater, 2015, 27, 4597

[5] Büchele P, Richter M, Tedde S F, et al. X-ray imaging with scintillator-sensitized hybrid organic photodetectors. Nat Photonics, 2015, 9, 843

[6] Kelley S O, Mirkin C A, Walt D R, et al. Advancing the speed, sensitivity and accuracy of biomolecular detection using multi-length-scale engineering. Nat Nanotechnol, 2014, 9, 969

[7] Qian L, Sun Y L, Wu M M, et al. A lead-free two-dimensional perovskite for a high-performance flexible photoconductor and a light-stimulated synaptic device. Nanoscale, 2018, 10, 6837

[8] Koppens F H L, Mueller T, Avouris P, et al. Photodetectors based on graphene, other two-dimensional materials and hybrid systems. Nat Nanotechnol, 2014, 9, 780

[9] Qu Y R, Li Q, Du K K, et al. Dynamic thermal emission control based on ultrathin plasmonic metamaterials including phase-changing material GST. Laser Photonics Rev, 2017, 11, 1770052

[10] Zhao Q Y, Zhu D, Calandri N, et al. Single-photon imager based on a superconducting nanowire delay line. Nat Photonics, 2017, 11, 247

[11] Geum D M, Kim S K, Lee S B, et al. Monolithic 3D integration of InGaAs photodetectors on Si MOSFETs using sequential fabrication process. IEEE Electron Device Lett, 2020, 41, 433

[12] Cao G Q, Wang F, Peng M, et al. Multicolor broadband and fast photodetector based on InGaAs-insulator-graphene hybrid heterostructure. Adv Electron Mater, 2020, 6, 1901007

[13] Zhai T Y, Li L, Ma Y, et al. One-dimensional inorganic nanostructures: Synthesis, field-emission and photodetection. Chem Soc Rev, 2011, 40, 2986

[14] Hsu S H. Reflectively coupled waveguide photodetector for high speed optical interconnection. Sensors, 2010, 10, 10863

[15] Casalino M, Coppola G, de la Rue R M, et al. State-of-the-art all-silicon sub-bandgap photodetectors at telecom and datacom wavelengths. Laser Photonics Rev, 2016, 10, 895

[16] Yu Y Q, Li Z, Lu Z J, et al. Graphene/MoS_2/Si nanowires Schottky-NP bipolar van der Waals heterojunction for ultrafast photodetectors. IEEE Electron Device Lett, 2018, 39, 1688

[17] Pyo S, Kim W, Jung H I, et al. Photodetectors: Heterogeneous integration of carbon-nanotube-graphene for high-performance, flexible, and transparent photodetectors. Small, 2017, 13, 1700918

[18] Dyson M J, Verhage M, Ma X, et al. Color determination from a single broadband organic photodiode. Adv Optical Mater, 2020, 8, 1901722

[19] Zhao Z J, Li C L, Shen L, et al. Photomultiplication type organic photodetectors based on electron tunneling injection. Nanoscale, 2020, 12, 1091

[20] Zhao Z J, Wang J, Xu C Y, et al. Photomultiplication type broad response organic photodetectors with one absorber layer and one multiplication layer. J Phys Chem Lett, 2020, 11, 366

[21] Chow P C Y, Someya T. Organic photodetectors for next-genera-

tion wearable electronics. Adv Mater, 2020, 32, e1902045
[22] Rezaei-Mazinani S, Ivanov A I, Proctor C M, et al. Monitoring intrinsic optical signals in brain tissue with organic photodetectors. Adv Mater Technol, 2018, 3, 1700333
[23] Li L, Chen H Y, Fang Z M, et al. An electrically modulated single-color/dual-color imaging photodetector. Adv Mater, 2020, 32, 1907257
[24] Shen L, Lin Y Z, Bao C X, et al. Integration of perovskite and polymer photoactive layers to produce ultrafast response, ultraviolet-to-near-infrared, sensitive photodetectors. Mater Horizons, 2017, 4, 242
[25] Pan J, Deng W, Xu X Z, et al. Photodetectors based on small-molecule organic semiconductor crystals. Chin Phys B, 2019, 28, 038102
[26] Li C L, Lu J R, Zhao Y, et al. Highly sensitive, fast response perovskite photodetectors demonstrated in weak light detection circuit and visible light communication system. Small, 2019, 15, e1903599
[27] Ren Y X, Dai T J, He B, et al. Fabrication of high-gain photodetector with graphene–PbSe heterostructure. IEEE Electron Device Lett, 2019, 40, 48
[28] Arredondo B, de Dios C, Vergaz R, et al. Performance of ITO-free inverted organic bulk heterojunction photodetectors: Comparison with standard device architecture. Org Electron, 2013, 14, 2484
[29] Wang W B, Zhang F J, Du M D, et al. Highly narrowband photomultiplication type organic photodetectors. Nano Lett, 2017, 17, 1995
[30] Kudo K, Moriizumi T. Spectrum-controllable color sensors using organic dyes. Appl Phys Lett, 1981, 39, 609
[31] Sariciftci N S, Braun D, Zhang C, et al. Semiconducting polymer-buckminsterfullerene heterojunctions: Diodes, photodiodes, and photovoltaic cells. Appl Phys Lett, 1993, 62, 585
[32] Yu G, Gao J, Hummelen J C, et al. Polymer photovoltaic cells: Enhanced efficiencies via a network of internal donor-acceptor heterojunctions. Science, 1995, 270, 1789
[33] Halls J J M, Walsh C A, Greenham N C, et al. Efficient photodiodes from interpenetrating polymer networks. Nature, 1995, 376, 498
[34] Rauch T, Böberl M, Tedde S F, et al. Near-infrared imaging with quantum-dot-sensitized organic photodiodes. Nat Photonics, 2009, 3, 332
[35] Han D, Khan Y, Ting J, et al. Pulse oximetry using organic optoelectronics under ambient light. Adv Mater Technol, 2020, 5, 1901122
[36] Huang J F, Lee J, Vollbrecht J, et al. A high-performance solution-processed organic photodetector for near-infrared sensing. Adv Mater, 2020, 32, 1906027
[37] Strobel N, Droseros N, Köntges W, et al. Color-selective printed organic photodiodes for filterless multichannel visible light communication. Adv Mater, 2020, 32, e1908258
[38] Kumar C, Jit S. Blended PQT-12 and PC61BM thin films based self-powered and fast response photodetector. IEEE Electron Device Lett, 2020, 41, 1556
[39] Ravi R, Deb B. Studies on one-step-synthesized hydrated vanadium pentoxide for efficient hole transport in organic photovoltaics. Energy Technol, 2020, 8, 1901323
[40] Karthik K, Nikolova M P, Phuruangrat A, et al. Ultrasound-assisted synthesis of V_2O_5 nanoparticles for photocatalytic and antibacterial studies. Mater Res Innov, 2020, 24, 229
[41] Torraca E, Costantino U, Massucci M A. Crystalline insoluble salts of polybasic metals: V. Ion-exchange properties of crystalline and amorphous zirconium arsenate. J Chromatograph A, 1967, 30, 584
[42] Kim B G, Ma X, Chen C, et al. Energy level modulation of HOMO, LUMO, and band-gap in conjugated polymers for organic photovoltaic applications. Adv Funct Mater, 2013, 23, 439
[43] Elgrishi N, Rountree K J, McCarthy B D, et al. A practical beginner's Guide to cyclic voltammetry. J Chem Educ, 2018, 95, 197
[44] Ji C H, Kim K T, Oh S Y. High-detectivity perovskite-based photodetector using a Zr-doped TiO_x cathode interlayer. RSC Adv, 2018, 8, 8302
[45] Tong S C, Yuan J, Zhang, C J et al. Large-scale roll-to-roll printed, flexible and stable organic bulk heterojunction photodetector. npj Flex Electron, 2018(1), 42
[46] Zeng Z, Zhong Z M, Zhong W K, et al. High-detectivity organic photodetectors based on a thick-film photoactive layer using a conjugated polymer containing a naphtho[1,2-*c*:5,6-*c*]bis[1,2,5]thiadiazole unit. J Mater Chem C, 2019, 7, 6070
[47] Sulaman M, Song Y, Yang S Y, et al. Interlayer of PMMA doped with Au nanoparticles for high-performance tandem photodetectors: A solution to suppress dark current and maintain high photocurrent. ACS Appl Mater Interfaces, 2020, 12, 26153
[48] Mahmood A. Photovoltaic and charge transport behavior of diketopyrrolopyrrole based compounds with A-D-A-D-a skeleton. J Clust Sci, 2019, 30, 1123
[49] Sulaman M, Song Y, Yang S Y, et al. Ultra-sensitive solution-processed broadband photodetectors based on vertical field-effect transistor. Nanotechnology, 2020, 31, 105203
[50] Imran A, Sulaman M, Yang S Y, et al. Molecular beam epitaxy growth of high mobility InN film for high-performance broadband heterointerface photodetectors. Surf Interfaces, 2022, 29, 101772
[51] Sulaman M, Song Y, Yang S Y, et al. High-performance solution-processed colloidal quantum dots-based tandem broadband photodetectors with dielectric interlayer. Nanotechnology, 2019, 30, 465203
[52] Mahmood A, Tang A L, Wang X C, et al. First-principles theoretical designing of planar non-fullerene small molecular acceptors for organic solar cells: Manipulation of noncovalent interactions. Phys Chem Chem Phys, 2019, 21, 2128
[53] Mahmood A, Khan S U D, Rana U A. Theoretical designing of novel heterocyclic azo dyes for dye sensitized solar cells. J Comput Electron, 2014, 13, 1033

Hemraj Dahiya is a Ph.D. Scholar in the Department of Physics at The LNM Institute of Information Technology, Jaipur, India, His main research interest is in the optoelectronic properties of organic materials for applications in photovoltaic devices. He is currently working on the non-fullerene-based third-generation organic solar cells.

Abhishek Kumar Singh is currently working as an Assistant Professor in the Department of Electronics Engineering at Rajiv Gandhi Institute of Petroleum Technology, in Jais, Amethi, Uttar Pradesh, India. He received the B.Tech. degree in electronics and communication engineering from the Faculty of Agriculture Engineering & Technology, CSA Kanpur, India, M.Tech. degree in optoelectronics and optical communication from the Indian Institute of Technology (IIT) Delhi, India, and a Ph.D. degree in the area of Microelectronics from the Indian Institute of Technology (BHU) Varanasi. He is currently working on experimental and theoretical research in the areas of microelectronics and photonics. His area of interest is fabrication, modeling, and simulation of electronic and optoelectronic devices, high-speed semiconductor devices (MESFETs), phototransistors, VLSI design for low power applications.